

# SAM-RL: Sensing-Aware Model-Based Reinforcement Learning via Differentiable Physics-Based Simulation and Rendering

Jun Lv<sup>1</sup>, Yunhai Feng<sup>2</sup>, Cheng Zhang<sup>3</sup>, Shuang Zhao<sup>3</sup>, Lin Shao<sup>4\*</sup> and Cewu Lu<sup>1\*</sup>

**Abstract**—Model-based reinforcement learning (MBRL) is recognized with the potential to be significantly more sample efficient than model-free RL. How an accurate *model* can be developed automatically and efficiently from raw sensory inputs (such as images), especially for complex environments and tasks, is a challenging problem that hinders the broad application of MBRL in the real world. In this work, we propose a sensing-aware model-based reinforcement learning system called *SAM-RL*. Leveraging the differentiable physics-based simulation and rendering, *SAM-RL* automatically updates the model by comparing rendered images with real raw images and produces the policy efficiently. With the sensing-aware learning pipeline, *SAM-RL* allows a robot to select an informative viewpoint to monitor the task process. We apply our framework to real-world experiments for accomplishing three manipulation tasks: robotic assembly, tool manipulation, and deformable object manipulation. We demonstrate the effectiveness of *SAM-RL* via extensive experiments. Supplemental materials and videos are available on our project webpage at <https://sites.google.com/view/sam-rl>.

## I. INTRODUCTION

Over the past decade, deep reinforcement learning (RL) has resulted in impressive successes, including mastering Atari games [1], winning the games of Go [2], and solving Rubik’s cube with a human-like robot hand [3]. However, deep RL algorithms adopt the paradigm of model-free RL and require vast amounts of training data, significantly limiting their practicality for real-world robotic tasks. Model-based reinforcement learning (MBRL) is recognized with the potential to be significantly more sample efficient than model-free RL [4]. How to automatically and efficiently develop an accurate *model* from raw sensory inputs (such as images), especially for complex environments and tasks, is a challenging problem that hinders the wide application of MBRL in the physical world.

One line of works [5–8] adopts representation learning approaches to learn the *model* from raw input data. They aim to learn low-dimensional latent states and action representations from high-dimensional input data like images. But the learned deep network might not satisfy the physical dynamics, and its quality may also significantly degenerate

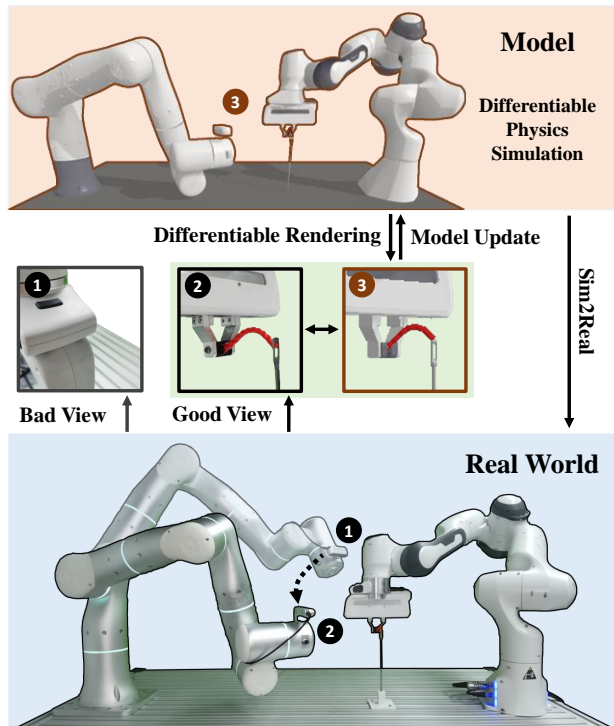


**Fig. 1:** Our proposed *SAM-RL* enables robots to autonomously select an informative camera viewpoint to better monitor the manipulation task (for example, the needle threading task). We leverage the differentiable rendering to update the model by comparing the raw observation between simulation and the real world, and differentiable physics simulation to produce policy efficiently.

beyond the training data distribution when testing in the wild. Recent developments in differentiable physics-based simulation [9–16] and rendering [17–20] provide an alternative direction to model the environment [21, 22]. Lv et al. [23] use differentiable physics-based simulation as the backbone of the *model* and train robots to perform articulated object manipulation in the real world. Their pipeline produces a file of Unified Robot Description Format (URDF) [24] of the environment, which is loaded into the differentiable simulation from raw point clouds gathered by an RGB-D camera mounted on its wrist. However, a sequence of camera poses is needed to scan the 3D environment every time step, and these camera poses are manually predefined, which is time-consuming and difficult to adapt to various tasks. Object colors and geometric details are not included in the *model*, limiting its representation capability [23].

By integrating differentiable physics-based simulation and rendering, we propose a sensing-aware model-based reinforcement learning system called *SAM-RL*. As shown in Fig. 1, we apply *SAM-RL* on a robot system with two

\*Equal advising.

<sup>1</sup>Jun Lv and Cewu Lu are with Department of Computer Science, Shanghai Jiao Tong University, China. [lyujune@sjtu.edu.cn, luewu@sjtu.edu.cn]

<sup>2</sup>Yunhai Feng are with the Department of Computer Science and Engineering, University of California San Diego, USA. [yuf020@ucsd.edu]

<sup>3</sup>Cheng Zhang and Shuang Zhao are with the Department of Computer Science, University of California Irvine, USA. [chengz20@uci.edu, shz@ics.uci.edu]

<sup>4</sup>Lin Shao is with the Department of Computer Science, National University of Singapore, Singapore. [linshao@nus.edu.sg]

7-DoF robotic arms (Flexiv [25] and Franka), where the former mounts an RGB-D camera, and the latter handles manipulation tasks. Our framework allows the robot to automatically select an informative camera view to effectively monitor the manipulation process, providing the following benefits. First, the system no longer requires obtaining a sequence of camera poses at each step, which is extremely time-consuming. Second, compared with using a fixed view, *SAM-RL* leverages varying camera views with potentially fewer occlusions and offers better estimations of environment states and object status (especially for deformable bodies). The improved quality in object status estimation contributes more effective robotic actions to complete various tasks. Third, by comparing rendered and measured (i.e., real-world) images, discrepancies between the simulation and the reality are better revealed and then reduced automatically using gradient-based optimization and differentiable rendering.

In practice, we train the robot to learn three challenging manipulation skills: peg-insertion, flipping a pancake with a spatula, and needle threading. Our experiments indicate that *SAM-RL* can significantly reduce training time and improve success rate by large margins compared to common model-free deep reinforcement learning algorithms.

Our primary contributions include: 1) proposing an active-sensing framework that enables robots to select the informative view for various manipulation tasks; 2) introducing a model-based reinforcement learning (MBRL) algorithm to produce efficient policies; 3) conducting extensive quantitative and qualitative evaluations to demonstrate the effectiveness of our approach; and 4) applying our framework to real-world robotic assembly, tool manipulation, and deformable object manipulation tasks.

## II. RELATED WORK

We review related literature on key components in our approach, including model-based reinforcement learning, next best view, integration of differentiable physics-based simulation and rendering, and robotic manipulation. We describe how we are different from previous work.

### A. Model-based Reinforcement Learning

MBRL is considered to be potentially more sample efficient than model-free RL [4]. However, automatically and efficiently developing an accurate model from raw sensory data is a challenging problem, which retards MBRL from being widely applied in the real world. For a broader review of the field on MBRL, we refer to [26]. One line of works [5–8] use representation learning methods to learn low-dimensional latent state and action representations from high-dimensional input data. But the learned models might not satisfy the physical dynamics, and the quality may also significantly drop beyond the training data distribution. Recently, Lv et al. [23] leveraged the differentiable physics simulation and developed a system to produce a URDF file to model the surrounding environment based on an RGB-D camera. However, the RGB-D camera poses used in [23] are predefined and can not adjust to different tasks. Our

approach allows the robot to select the most informative camera view to monitor the manipulation process and update the environment model automatically.

### B. Next Best View in Active Sensing

Next Best View (NBV) has been one of the core problems in active sensing. It studies the problem of how to obtain a series of sensor poses to increase the ‘information gain’. The ‘information gain’ are explicitly defined to reflect the improved perception for 3D reconstruction [27–30], object recognition [31–34], 3D model completion [35], pose estimation, and 3D exploration [36, 37]. Unlike perception-related tasks, we explore the NBV over a wide range of robotic manipulation tasks. ‘Information gain’ in the robotic manipulation tasks is difficult to define explicitly and is implicitly related to task performance. In our system, the environment changes accordingly after the robot’s interaction. We integrate the ‘information gain’ into the  $Q$  function under the setting of partially observable Markov decision processes (POMDPs).

### C. Integration of Differentiable Physics-Based Simulation and Rendering

Recently, great progresses have been made in the field of differentiable physics-based simulation and rendering. For a broader review, please refer to [9–16] and [38, 39]. With the development of these techniques, Jatavallabhula et al. [21] first proposed a pipeline to leverage differentiable simulation and rendering for system identification and visuomotor control. Ma et al. [22] introduced a rendering-invariant state predictor network that maps images into states agnostic to rendering parameters. By comparing the state predictions obtained using rendered and ground-truth images, the pipeline can backpropagate the gradient to update system parameters and actions. Sundaresan et al. [40] proposed a real-to-sim parameter estimation approach from point clouds for deformable objects. Different from these works, we use the differentiable simulation and rendering to find the next best view for various manipulation tasks and update the object status in the *model* by comparing rendered and captured images.

### D. Manipulation

Our framework can be adopted to improve the performance of a range of manipulation tasks. We review the related work in these domains. 1) *Peg-insertion*. Peg insertion is a classic robotic assembly task with rich literature [41–43]. For a broad review of peg-insertion, we refer to [44]. 2) *Spatula Flipping*. Chebotar et al. [45] used the tactile sensor to train the robot learning to perform a scraping task with a spatula. Tsuji et al. [46] studied the dynamic object manipulation by a spatula. They clarified the conditions for achieving dynamic movements and presented a unified algorithm for generating a variety of movements. 3) *Needle Threading*. Silv  rio et al. [47] relied on a high-resolution laser scanner to perceive the thread and needle. Huang et al. [48] used a high-speed camera to monitor the process and provide high-speed visual feedback. Kim et al. [49] proposed

a deep imitation learning algorithm for the needle threading task. Unlike approaches above, we develop a sensing-aware model-based reinforcement learning approach to learn these skills.

### III. TECHNICAL APPROACH

Given a manipulation task denoted as  $\mathcal{T}$ , our pipeline takes as input images gathered from an RGB-D camera and outputs a policy to select the camera pose  $\mathcal{P}$  followed by producing an action  $a$ . An overview of our proposed method is shown in Fig. 2. In what follows, we first briefly introduce the model  $\mathcal{M}$  that integrates differentiable physics-based simulation and rendering in Sec. III-A. Then, we describe developing and updating the model in  $\mathcal{M}$  (Real2Sim) in Sec. III-B, training robots to learn the perception and action with the *model* (Learn@Sim) in Sec. III-D, and applying the learned *model* to the real world (Sim2Real) in Sec. III-C.

#### A. Model with differentiable simulation and rendering

In this work, we combine the differentiable physics-based simulation and rendering. The resulting differentiable system plays the backbone of the *model*, which we denote as  $\mathcal{M}$ , for the model-based reinforcement learning. The model can load robots, cameras, and objects denoted as  $\{\mathcal{O}_j^{sim}\}$  along with their visual/geometric (e.g., shape, pose, and color) and physical attributes (e.g., mass, inertial, and friction coefficient). We denote the attributes of all objects loaded in the simulation as one type of model's parameters  $\psi_{\mathcal{M}}$  as follows:

$$\psi_{\mathcal{M}} = \sum_j \mathcal{O}_j^{sim}. \quad (1)$$

The *model* can render an image  $\mathcal{I}^{sim} = \mathcal{M}(\psi_{\mathcal{M}}, \mathcal{P}; \text{render})$  under the camera pose  $\mathcal{P}$ . We can get the gradient of  $\partial \mathcal{I}^{sim} / \partial \mathcal{P}$  and  $\partial \mathcal{I}^{sim} / \partial \mathcal{O}_j^{sim}$  using differentiable rendering. Note that  $\partial \mathcal{I}^{sim} / \partial \mathcal{O}_j^{sim}$  contains only the gradient with respect to object visual/geometric attributes.

Additionally, given the state  $s_t^{sim}$  including the object attributes  $\psi_{\mathcal{M}}$  and the robots' status, when an action denoted as  $a_t^{sim}$  is executed (for example, an external force is exerted on the object), the model simulates the next state  $s_{t+1}^{sim} = \mathcal{M}(s_t^{sim}, a_t^{sim}; \text{forward})$  in a differentiable fashion, providing the gradients  $\partial s_{t+1}^{sim} / \partial a_t^{sim}$  and  $\partial s_{t+1}^{sim} / \partial s_t^{sim}$ .

#### B. Real2Sim: developing model from the real world

1) *Build the initial Model*: For model-based reinforcement learning, the first step is to build an initial *model* of the environment. The initial *model* does not need to be accurate and can be created using current 3D object reconstruction methods with RGB-D cameras like BundleFusion [50], KinectFusion [51]. In our setting, as shown in Fig. 2, a calibrated RGB-D camera is mounted on the robot's wrist. Therefore the robot system takes a set of images with corresponding accurate camera poses. The initial *model* can also be built directly from a CAD model [52] or following the pipeline to produce the URDF described in SAGCI [23]. After the initialization, the model  $\mathcal{M}$  contains the robots, objects and an RGB-D camera.

2) *Update the Model with differentiable Rendering*: After having an initial *model*, we then describe how to update the *model* by directly comparing the raw visual observation in simulation and the real world, leveraging the differentiable rendering[53]. In this work, we only care about one object and assume we can get accurate object segmentation of real world images. With common techniques such as Mask R-CNN [54], it's feasible to get a fine object-level instance segmentation.

At each time step  $t$ , we update the camera and robot pose in simulation to match the corresponding camera and robot pose in the real world. Then we get the rendered RGB-D image from  $\mathcal{M}$  and corresponding real RGB-D image with associated segmentation. Based on the camera parameters, we transform the depth image to point cloud and segment the point cloud. We denote the RGB image, associated object segmentation, and segmented point cloud  $(\mathcal{I}^{sim,rgb}, \mathcal{G}^{sim}, \mathcal{X}^{sim})$  in the simulation and  $(\mathcal{I}^{real,rgb}, \mathcal{G}^{real}, \mathcal{X}^{real})$  in the real world. For simplicity, we use  $\mathcal{I}^{sim}$  to represent the  $(\mathcal{I}^{sim,rgb}, \mathcal{G}^{sim}, \mathcal{X}^{sim})$  and  $\mathcal{I}^{real}$  is defined accordingly.

We define the loss functions as follows.

$$\mathcal{L}_1 = \|\mathcal{G}^{real} \otimes \mathcal{I}^{real,rgb} - \mathcal{G}^{sim} \otimes \mathcal{I}^{sim,rgb}\|_1 \quad (2)$$

$$\mathcal{L}_2 = \text{EMD}(\mathcal{X}^{sim}, \mathcal{X}^{real}) \quad (3)$$

$$\mathcal{L} = \lambda_1 \mathcal{L}_1 + \lambda_2 \mathcal{L}_2 \quad (4)$$

where  $\otimes$  represents the pixel-wise product operator and *EMD* represents the Earth Mover Distance [55] to measure the distance between two 3D point clouds. Note that  $(\mathcal{I}^{sim,rgb}, \mathcal{G}^{sim}, \mathcal{X}^{sim}) = \mathcal{M}(\psi_{\mathcal{M}}, \mathcal{P}; \text{render})$  as explained in Sec. III-A, whose process is differentiable. With the gradient  $\partial \mathcal{L} / \partial \psi_{\mathcal{M}}$ , we can update the model  $\mathcal{M}$ 's parameters  $\psi_{\mathcal{M}}$  including object mesh vertices, colors, and 6D pose (for articulated/rigid objects) so that the loss  $\mathcal{L}$  is reduced.

$$\psi_{\mathcal{M}} \leftarrow \psi_{\mathcal{M}} - \lambda_{\mathcal{M}} \frac{\partial \mathcal{L}}{\partial \psi_{\mathcal{M}}} \quad (5)$$

Through this, we can keep reducing the discrepancy between the simulation and the real world, making the model more and more accurate.

Up to now, we have introduced how to build and update the model. Due to the page limit, we report the detailed pipeline in the supplementary.

#### C. Sim2Real: learning residual policy in the real world

We delay the discussion of how to learn the policy to complete the task  $\mathcal{T}$  with the *model* to the next subsection III-D. Here we assume that we have the policy  $\pi^{sim}$  in simulation which takes rendered images  $\mathcal{I}^{sim}$  as inputs and outputs actions denoted as  $a^{sim} = \pi^{sim}(\mathcal{I}^{sim})$ . We describe how to apply the learned policy from simulation to the real world by learning a residual policy  $\pi^{res}$ .

We set the same camera pose denoted as  $\mathcal{P}$  both in the simulation and the real world and get images denoted as  $\mathcal{I}^{sim,0}$  and  $\mathcal{I}^{real}$ . We first update the *model*'s parameter  $\psi_{\mathcal{M}}$  by minimizing the loss with Eqn. 1 as described in Sec. III-B.2 and then get the new images  $\mathcal{I}^{sim}$  with the updated  $\psi_{\mathcal{M}}$ .

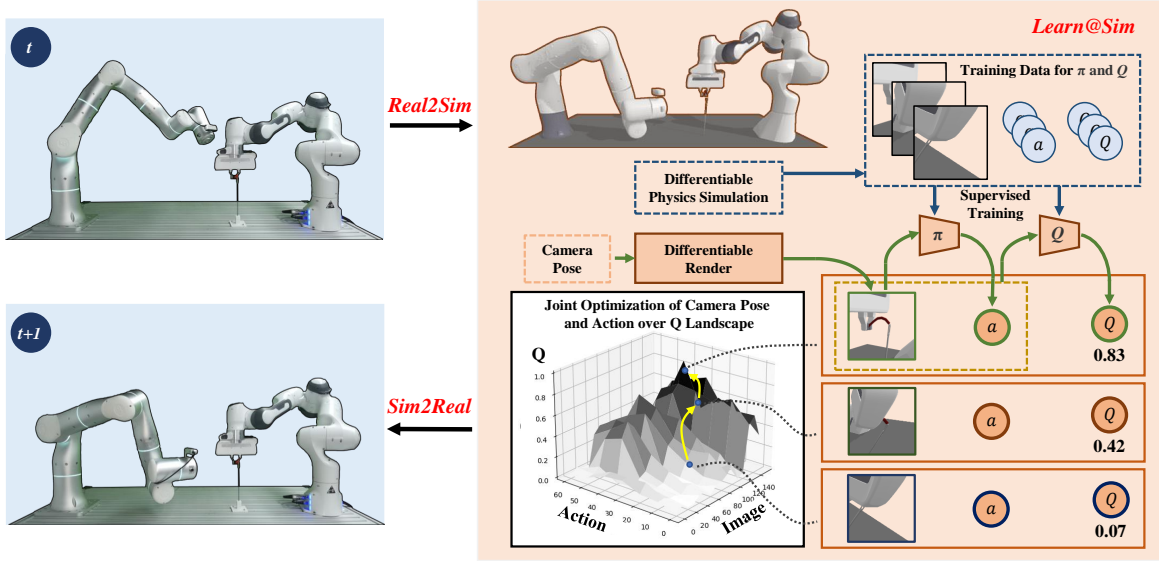


**Fig. 2:** The overall approach of SAM-RL includes Real2Sim, Learn@Sim, and Sim2Real stages. SAM-RL automatically develop the *model* during Real2Sim stage. During the Learn@Sim stage, it learns the sensing-aware Q function and actor  $\pi^{sim}$  in the *model*. The differentiable physics simulation generates training data (rendered image, action, and associated return) to learn the Q function and actor function, which allows the robot to select an informative view. In the Sim2Real stage, SAM-RL learns a residual policy to reduce the sim2real gap.

With the  $\mathcal{I}^{sim}$  and  $\mathcal{I}^{real}$ , we get an action from simulation  $a^{sim} = \pi^{sim}(\mathcal{I}^{sim})$ . Instead of directly applying the action  $a^{sim}$  in the real world, we send the real image and the  $a^{sim}$  to the actor model in the real world to get the action as follows.

$$a^{real} = \pi^{real}(\mathcal{I}^{real}, a^{sim}) = a^{sim} + \pi^{res}(\mathcal{I}^{real}, a^{sim}) \quad (6)$$

We receive the reward  $r^{real}$ , whether the task succeeds *done*, and the next image  $\mathcal{I}^{real'}$ . Store the  $(\mathcal{I}^{real}, a^{real}, a^{sim}, r^{real}, done, \mathcal{I}^{real'})$  to the reply buffer to update the  $\pi^{real}$  following the common deep reinforcement learning procedures [52, 56]. Due to the page limit, we report the detailed training pipeline in the supplementary.

#### D. Learn@Sim: learning sensing-aware action in simulation

With the *model*, we discuss how to learn the informative camera pose  $\mathcal{P}$  associated with the rendered image  $\mathcal{I}^{sim}$  and action  $a^{sim}$  to complete the given task  $\mathcal{T}$  in the simulation.

1) *Sensing-aware Q-function:* We adopt the Q function  $Q^{sim}(\mathcal{I}^{sim}, a^{sim})$  to reflect the informative viewpoint. We can calculate the gradient of Q with respect to the camera pose  $\mathcal{P}$  as follows.

$$\frac{\partial Q^{sim}(\mathcal{I}^{sim}, a^{sim})}{\partial \mathcal{P}} = \frac{\partial Q^{sim}(\mathcal{I}^{sim}, a^{sim})}{\partial \mathcal{I}^{sim}} \frac{\partial \mathcal{I}^{sim}}{\partial \mathcal{P}} \quad (7)$$

Here the first term  $\partial Q^{sim} / \partial \mathcal{I}^{sim}$  is available through the backward propagation of the neural network. The second term  $\partial \mathcal{I}^{sim} / \partial \mathcal{P}$  can be obtained from the differentiable renderer [18]. The gradient of  $\partial Q^{sim} / \partial \mathcal{P}$  provides information on how to find a more informative viewpoint. Under the more informative viewpoint, the actor have a better sense of the state to generate an action associated with a higher Q value. We verify our hypothesis by visualizing the learned Q function in Sec IV-B.2.

Note that  $Q^{sim}(\mathcal{I}^{sim}, a^{sim})$  is defined under the setting of partially observable Markov decision processes (POMDPs) instead of Markov decision processes (MDPs). In POMDPs, the true state  $s_t$  is not fully observable, and a belief  $b_t$  is used to estimate the current state. A POMDP is formulated as an MDP defined over belief states [57]. In our case, we learn a function to approximate  $b_t$  from  $\mathcal{I}_t$  and the Q function is defined over belief state  $b^{sim}$  instead of the  $s^{sim}$  as shown in  $Q(\mathcal{I}^{sim}, a^{sim}) \approx Q(b^{sim}, a^{sim}) \neq Q(s^{sim}, a^{sim})$ .

2) *Learning actor in simulation to reflect the sensing quality in the real world:* In this part, we discuss how we learn an actor  $\pi^{sim}$  in simulation, which takes rendered image  $\mathcal{I}^{sim}$  and outputs the action. The actor  $\pi^{sim}$  is developed to imitate the sensing quality of  $\pi^{real}$  in the real world due to occlusion or object deformation. Images under different camera views might have different occlusions or object deformation status estimations. These variations in sensing quality also affect the actor's performances. We are using the performances of  $\pi^{sim}$  to reflect the performances of  $\pi^{real}$ .

There are multiple ways to learn the  $\pi^{sim}$  in the simulation via reinforcement learning or imitation learning. In this work, we choose the imitation learning approach (DAGger algorithm [58]) to learn the  $\pi^{sim}$ , which we find effective and efficient. With the *model*  $\mathcal{M}$  built with the differentiable physics simulation [10], our pipeline generates trajectories denoted as  $\{(s_t^{sim}, a_t^{sim} | \mathcal{T})\}_{t=1}^T$  to complete the task. For how to efficiently generate the trajectories inside the differentiable physics simulation, we put the detailed description of the process in the supplementary due to page limit.

After gathering these successful trajectories  $\{(s_t^{sim}, a_t^{sim} | \mathcal{T})\}_{t=1}^T$  in the simulation, we rendered multiple images  $\{\mathcal{I}_t^{sim}(\mathcal{P}^i)\}$  for each state  $s_t^{sim}$  under different camera poses  $\{\mathcal{P}^i\}$ . We train an actor  $\pi^{sim}(\mathcal{I}_t(s_t^{sim}, \mathcal{P}^i))$

to predict the action  $\hat{a}_t^{sim}$  to imitate the corresponding action  $a_t^{sim}$ . In the process, the prediction error is defined as follows

$$L^{\pi^{sim}} = \|\hat{a}_t^{sim} - a_t^{sim}\| \quad (8)$$

During the learning process, the prediction error also depends on the sensing quality. Our hypothesis is the actor might not learn the effective ground-truth action if there is insufficient state information in the rendered image. For example, if the camera is always looking into the sky and the object does not appear in the rendered image, it will be difficult for the actor to learn the correct action. We visualize the prediction error and put the visualization example in the supplementary. Note that the learning process also generates success and failure trajectories denoted as  $(\mathcal{I}_t^{sim}, \hat{a}_t^{sim})$ , which are used to learn the  $Q$  function.

3) *Learning sensing-aware  $Q$  function:* Here we describe how to learn the sensing-aware  $Q$  function denoted as  $Q^{sim}(\mathcal{I}^{sim}, a^{sim})$ . There are also multiple ways to learn the  $Q$  function. In this work, we formulate it as a supervised learning problem. We roll out the trajectories in the simulation to generate the training data. Given a trajectory  $\{(\mathcal{I}_t^{sim}(\mathcal{P}_t^i), \hat{a}_t^{sim})\}_{t=1}^T$ , we calculate the return  $\mathcal{R}_t = \sum_{i=t}^T \gamma^{T-i} r_i$  associated with each image and action pair, where  $r_t$  is the reward and  $\gamma$  is the discount factor. We then train a deep network that takes  $\mathcal{I}_t^{sim}$  and  $\hat{a}_t^{sim}$  as inputs and outputs the  $Q$  value by minimizing the following loss.

$$\mathcal{L}^Q = \|Q^{sim}(\mathcal{I}_t^{sim}, \hat{a}_t^{sim}) - \mathcal{R}_t\|_2 \quad (9)$$

4) *selecting perception and action leveraging the actor and  $Q$ -function:* Starting from an initial viewpoint  $\mathcal{P}$ , the simulation rendered an image  $\mathcal{I}^{sim}$ . We feed the image into the actor model to get an action  $a^{sim} = \pi^{sim}(\mathcal{I}^{sim})$ , and then send the image and action to the  $Q$  function to get the value  $Q^{sim}(\mathcal{I}^{sim}, a^{sim})$ . We get the gradient with respect to the  $\mathcal{P}$  and update the camera pose as follows.

$$\mathcal{P}' = \mathcal{P} + \lambda \frac{\partial Q^{sim}(\mathcal{I}^{sim}, a^{sim})}{\partial \mathcal{P}} \quad (10)$$

With the new camera pose  $\mathcal{P}'$ , we gather the new rendered image  $\mathcal{I}^{sim'}$  and associated  $Q^{sim}(\mathcal{I}^{sim'}, a^{sim'})$ . We accept the new camera pose and new action if  $Q(\mathcal{I}^{sim'}, a^{sim'}) \geq Q(\mathcal{I}^{sim}, a^{sim})$ .

We summarize the overall test stage pipeline in the following Alg. 1 and put the overall training algorithm in the supplementary due to page limit.

#### IV. EXPERIMENTS

Our experiments focus on evaluating the following questions: 1) Can our proposed selecting perception and action procedure described at III-D.4 improve the performance of various manipulation tasks? 2) How does our *SAM-RL* approach compare with model-free deep reinforcement learning algorithms? 3) How effective is each component in our proposed *SAM-RL* algorithm?

#### Algorithm 1: Overall algorithm in test stage

---

**Input:** the model  $\mathcal{M}$  with its model parameters  $\psi_{\mathcal{M}}$ , camera pose  $\mathcal{P}$ , take the real image using real camera  $Cam(\mathcal{P})$

```

1 for  $t$  in each iteration do
2    $\mathcal{I}^{sim} \leftarrow \mathcal{M}(\psi_{\mathcal{M}}, \mathcal{P}; render)$ ,  $\mathcal{I}^{real} \leftarrow Cam(\mathcal{P})$ ;
3   Update  $\psi_{\mathcal{M}}$  by reducing  $\|\mathcal{I}^{sim} - \mathcal{I}^{real}\|$ ;
4    $\mathcal{I}^{sim} \leftarrow \mathcal{M}(\psi_{\mathcal{M}}, \mathcal{P}; render)$ ,  $a^{sim} = \pi^{sim}(\mathcal{I}^{sim})$ ;
5   while True do
6      $\mathcal{P}' = \mathcal{P} + \lambda \frac{\partial Q(\mathcal{I}^{sim}, a^{sim})}{\partial \mathcal{P}}$ ;
7      $\mathcal{I}^{sim'} \leftarrow \mathcal{M}(\psi_{\mathcal{M}}, \mathcal{P}'; render)$ ,  $\mathcal{I}^{real'} \leftarrow Cam(\mathcal{P}')$ ;
8     Update  $\psi_{\mathcal{M}}$  by reducing  $\|\mathcal{I}^{sim'} - \mathcal{I}^{real'}\|$ ;
9      $\mathcal{I}^{sim'} \leftarrow \mathcal{M}(\psi_{\mathcal{M}}, \mathcal{P}'; render)$ ,  $a^{sim'} = \pi^{sim}(\mathcal{I}^{sim'})$ ;
10    if  $Q^{sim}(\mathcal{I}^{sim}, a^{sim}) \leq Q^{sim}(\mathcal{I}^{sim'}, a^{sim'})$  then
11       $\mathcal{I}^{real} \leftarrow \mathcal{I}^{real'}$ ,  $a^{sim} \leftarrow a^{sim'}$ ;
12      break;
13    end
14     $\mathcal{I}^{sim} \leftarrow \mathcal{I}^{sim'}$ ,  $\mathcal{P} \leftarrow \mathcal{P}'$ ,  $a^{sim} \leftarrow a^{sim'}$ ;
15  end
16   $a^{real} = \pi^{real}(\mathcal{I}^{real}, a^{sim})$ ;
17  Execute the action  $a^{real}$  both in the real world and in simulation;
18 end

```

---

#### A. Experimental Setup

1) *Manipulation Tasks:* We design three different manipulation tasks as shown in Fig. 3: inserting a peg into a hole (*Peg-Insertion*), flipping a pancake with a spatula (*Spatula-Flipping*), and threading a needle (*Needle-Threading*). The *Peg-Insertion* task is considered successful if the peg is inserted into the hole. The *Spatula-Flipping* is successful if the pancake is lifted up by the spatula and then flipped. The *Needle-Threading* is successful if the thread is put through the needle's hole.

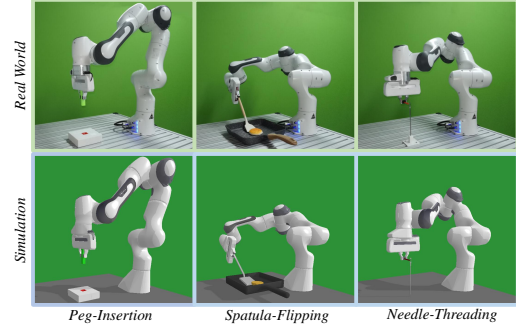


**Fig. 3:** Visualization of experiment setup for *Peg-Insertion*, *Spatula-Flipping*, and *Needle-Threading*.

2) *Real World:* We set up the real world experiment with two 7 DoF robotic arms as shown in Fig 1. One robot is the Franka Panda performing the manipulation task. The other robot is Flexiv [25] holding the RGB-D RealSense camera. We calibrate the camera intrinsic matrix and the hand-eye transformation between the camera and the Flexiv's end-effector. We also measure the relative transformation between two robots' bases in the world coordinate.

3) *Simulation:* In the simulation, we set the camera intrinsic matrix and relative transformations of the camera to Flexiv and Flexiv to Franka based on the real-world calibration results. We use PyBullet [59] to simulate the real world, which is different from our differentiable physics simulation for quantitative experiments. Objects are initialized with a random pose within manually defined bounds. Due to the



page limit, we put the detailed description of the simulation in the supplementary.

### B. Evaluating the sensing-aware function

1) *Quantitative Results*: To evaluate the learned sensing-aware  $Q$  function during Learn@Sim stage, we set up the following experiments inside the differentiable physics simulation. We use the same actor model  $\pi^{sim}$  trained with rendered images under multiple camera views, and evaluate the actor with and without leveraging the sensing-aware  $Q$  function to optimize the camera pose during manipulation processes, denoted as *Ours* and *Ours(w/o pose-opt)*, respectively. We also train the same actor with rendered images under a fixed camera view, and evaluate the trained actor under the same camera view, denoted as *Fixed-View*. To make relatively fair comparison, we train the actor in *Fixed-View* to have the same prediction error in the training process as in *Ours*. We report the task success rate under these three settings. As shown in Tab. I, our pipeline can find the informative view to benefit robot manipulation with the sensing-aware  $Q$  function.

**TABLE I:** Quantitative results of sensing-aware  $Q$  function.

	<i>Ours</i>	<i>Ours(w/o pose-opt)</i>	<i>Fixed View</i>
<i>Peg Insertion</i>	<b>0.82</b>	0.64	0.71
<i>Spatula Flipping</i>	<b>0.65</b>	0.57	0.55
<i>Needle Threading</i>	<b>0.70</b>	0.46	0.66

2) *Qualitative Visualization*: We visualize the learned  $Q$  function for the *Needle-Threading* task in Fig. 4. We gather rendered images  $\mathcal{I}^{sim}(\mathcal{P}^i)$  from multiple view points and send them to the actor  $\pi^{sim}$  to get associated actions  $\pi^{sim}(\mathcal{I}^{sim}(\mathcal{P}^i))$ , and get the  $Q$  values  $Q^{sim}(\mathcal{I}^{sim}(\mathcal{P}^i), \pi^{sim}(\mathcal{I}^{sim}(\mathcal{P}^i)))$ . It indicates that our  $Q$  function learns a reasonable policy to select the camera viewpoint.

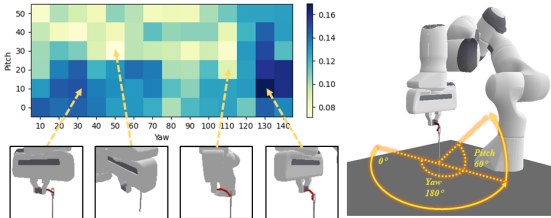
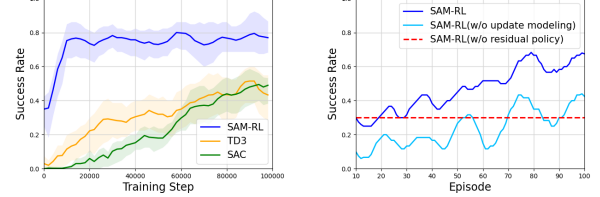


**Fig. 4:** Qualitative visualization of sensing-aware  $Q$  function for the *Needle Threading*. Each pixel corresponds to a yaw and pitch value of the camera view.

### C. Comparing the SAM-RL with model-free deep RL

We compare our *SAM-RL* with common model-free DRL algorithm *TD3* [60] and *SAC* [56]. In this experiment, we adopt pybullet as the “real world”. For *TD3* and *SAC*, we directly train the robot in pybullet. Due to the page limit, we put the definitions of the observation, action, and reward functions in the supplementary. For *SAM-RL*, we develop the *model* via the differentiable physics-based simulation and rendering and use the *model* to complete tasks in pybullet (“real world”). Every time the environment is initialized or reset, the position and shape of the thread are randomly set within a certain range. Fig. 5(a) shows the

average success rate of the *SAC* and *TD3* during the training stage. After training 100k steps, the average success rate of *SAC* models and *TD3* models are about 50%. However, our pipeline achieves a success rate of around 80% after 8k training steps. It indicates that our proposed *SAM-RL* is significantly sample-efficient compared to model-free deep reinforcement learning approaches.



(a) Comparison with model-free deep RL in simulation (b) Ablation studies in the real world

**Fig. 5:** Learning Curves of the *Needle Threading*. The x-axis shows the training steps/episodes and y-axis indicates the success rate.

### D. Ablation: Evaluating components of SAM-RL

We apply *SAM-RL* in the real robot system and conduct two ablation study experiments. **A1**: We remove the component of updating the *model*  $\mathcal{M}$  by comparing  $\mathcal{I}^{real}$  and  $\mathcal{I}^{real}$  and denote the experiment as *SAM-RL (w/o update modeling)*. **A2**: We remove the residual policy used to address the sim2real gap and directly execute the predicted action  $a^{sim}$  in the real world denoted as *SAM-RL (w/o residual policy)*. We post the result of *Needle Threading* in Fig. 5(b), and more results on other tasks and detailed experiment descriptions are put in the supplementary due to page limit. Fig. 5(b) shows that these components play important roles in our pipeline, and removing these components results in significant performance decreases.

### E. Evaluating the model updating via differentiable rendering

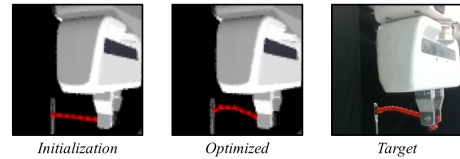


**Fig. 6:** The rightmost image is the real image, the target image for model update. The leftmost image and middle image show the initial state of the thread and the updated thread leveraging the differentiable rendering. More examples are available on the project webpage.

## V. CONCLUSION

We propose a sensing-aware model-based reinforcement learning called *SAM-RL* leveraging the differentiable physics-based simulation and rendering. *SAM-RL* automatically updates the model by comparing the raw observations between simulation and the real world, and produces the policy efficiently. It also allows robots to select an informative viewpoint to better monitor the task process. We apply the system to robotic assembly, tool manipulation, and deformable object manipulation tasks. Extensive experiments in the simulation and the real world demonstrate the effectiveness of our proposed learning framework.

# REFERENCES

- [1] V. Mnih, K. Kavukcuoglu, D. Silver, A. A. Rusu, J. Veness, M. G. Bellemare, A. Graves, M. Riedmiller, A. K. Fidjeland, G. Ostrovski *et al.*, “Human-level control through deep reinforcement learning,” *nature*, vol. 518, no. 7540, pp. 529–533, 2015.
- [2] D. Silver, A. Huang, C. J. Maddison, A. Guez, L. Sifre, G. van den Driessche, J. Schrittwieser, I. Antonoglou, V. Panneershelvam, M. Lanctot, S. Dieleman, D. Grewe, J. Nham, N. Kalchbrenner, I. Sutskever, T. Lillicrap, M. Leach, K. Kavukcuoglu, T. Graepel, and D. Hassabis, “Mastering the game of go with deep neural networks and tree search,” *Nature*, vol. 529, pp. 484–503, 2016.
- [3] I. Akkaya, M. Andrychowicz, M. Chociej, M. Litwin, B. McGrew, A. Petron, A. Paino, M. Plappert, G. Powell, R. Ribas *et al.*, “Solving rubik’s cube with a robot hand,” *arXiv preprint arXiv:1910.07113*, 2019.
- [4] T. Wang, X. Bao, I. Clavera, J. Hoang, Y. Wen, E. Langlois, S. Zhang, G. Zhang, P. Abbeel, and J. Ba, “Benchmarking model-based reinforcement learning,” *arXiv preprint arXiv:1907.02057*, 2019.
- [5] M. Yang and O. Nachum, “Representation matters: offline pretraining for sequential decision making,” in *International Conference on Machine Learning*. PMLR, 2021, pp. 11 784–11 794.
- [6] D. Hafner, T. Lillicrap, J. Ba, and M. Norouzi, “Dream to control: Learning behaviors by latent imagination,” *arXiv preprint arXiv:1912.01603*, 2019.
- [7] D. Hafner, T. Lillicrap, I. Fischer, R. Villegas, D. Ha, H. Lee, and J. Davidson, “Learning latent dynamics for planning from pixels,” in *International conference on machine learning*. PMLR, 2019, pp. 2555–2565.
- [8] D. Hafner, T. Lillicrap, M. Norouzi, and J. Ba, “Mastering atari with discrete world models,” *arXiv preprint arXiv:2010.02193*, 2020.
- [9] Y. Hu, L. Anderson, T.-M. Li, Q. Sun, N. Carr, J. Ragan-Kelley, and F. Durand, “DiffTaichi: Differentiable programming for physical simulation,” *ICLR*, 2020.
- [10] K. Werling, D. Omens, J. Lee, I. Exarchos, and C. K. Liu, “Fast and feature-complete differentiable physics for articulated rigid bodies with contact,” in *Proceedings of Robotics: Science and Systems (RSS)*, July 2021.
- [11] T. A. Howell, S. Le Cleac’h, J. Z. Kolter, M. Schwager, and Z. Manchester, “Dojo: A Differentiable Simulator for Robotics,” *Robotics: Science and Systems 2022*, Mar. 2022, under review. [Online]. Available: <http://arxiv.org/abs/2203.00806>
- [12] T. Du, K. Wu, P. Ma, S. Wah, A. Spielberg, D. Rus, and W. Matusik, “Diffpd: Differentiable projective dynamics,” *ACM Trans. Graph.*, vol. 41, no. 2, nov 2021. [Online]. Available: <https://doi.org/10.1145/3490168>
- [13] Y. Li, T. Du, K. Wu, J. Xu, and W. Matusik, “Diffcloth: Differentiable cloth simulation with dry frictional contact,” *ACM Trans. Graph.*, mar 2022, just Accepted. [Online]. Available: <https://doi.org/10.1145/3527660>
- [14] Y. Qiao, J. Liang, V. Koltun, and M. Lin, “Differentiable simulation of soft multi-body systems,” *Advances in Neural Information Processing Systems*, vol. 34, pp. 17 123–17 135, 2021.
- [15] Y.-L. Qiao, J. Liang, V. Koltun, and M. C. Lin, “Scalable differentiable physics for learning and control,” *arXiv preprint arXiv:2007.02168*, 2020.
- [16] J. Liang, M. Lin, and V. Koltun, “Differentiable cloth simulation for inverse problems,” *Advances in Neural Information Processing Systems*, vol. 32, 2019.
- [17] S. Liu, T. Li, W. Chen, and H. Li, “Soft rasterizer: A differentiable renderer for image-based 3d reasoning,” in *Proceedings of the IEEE/CVF International Conference on Computer Vision*, 2019, pp. 7708–7717.
- [18] T.-M. Li, M. Aittala, F. Durand, and J. Lehtinen, “Differentiable monte carlo ray tracing through edge sampling,” *ACM Trans. Graph. (Proc. SIGGRAPH Asia)*, vol. 37, no. 6, pp. 222:1–222:11, 2018.
- [19] C. Zhang, B. Miller, K. Yan, I. Gkioulekas, and S. Zhao, “Path-space differentiable rendering,” *ACM Trans. Graph.*, vol. 39, no. 4, pp. 143:1–143:19, 2020.
- [20] S. P. Bangaru, T.-M. Li, and F. Durand, “Unbiased warped-area sampling for differentiable rendering,” *ACM Trans. Graph.*, vol. 39, no. 6, pp. 245:1–245:18, 2020.
- [21] K. M. Jatavallabhula, M. Macklin, F. Golemo, V. Voleti, L. Petrini, M. Weiss, B. Considine, J. Parent-Levesque, K. Xie, K. Erleben, L. Paull, F. Shkurti, D. Nowrouzezahrai, and S. Fidler, “gradsim: Differentiable simulation for system identification and visuomotor control,” *International Conference on Learning Representations (ICLR)*, 2021. [Online]. Available: [https://openreview.net/forum?id=c\\_E8kFWfhp0](https://openreview.net/forum?id=c_E8kFWfhp0)
- [22] P. Ma, T. Du, J. B. Tenenbaum, W. Matusik, and C. Gan, “Risp: Rendering-invariant state predictor with differentiable simulation and rendering for cross-domain parameter estimation,” in *International Conference on Learning Representations*, 2021.
- [23] J. Lv, Q. Yu, L. Shao, W. Liu, W. Xu, and C. Lu, “Sagci-system: Towards sample-efficient, generalizable, compositional, and incremental robot learning,” in *2022 IEEE International Conference on Robotics and Automation (ICRA)*. IEEE, 2022.
- [24] R. ROS, “urdf,” <http://wiki.ros.org/urdf>, 2020.
- [25] F. R. Inc., “Flexiv robot arm,” 2019. [Online]. Available: <https://www.flexiv.com/en/application>
- [26] F.-M. Luo, T. Xu, H. Lai, X.-H. Chen, W. Zhang, and Y. Yu, “A survey on model-based reinforcement learning,” *arXiv preprint arXiv:2206.09328*, 2022.
- [27] C. Collander, W. J. Beksi, and M. Huber, “Learning the next best view for 3d point clouds via topological features,” in *2021 IEEE International Conference on Robotics and Automation (ICRA)*. IEEE, 2021, pp. 12 207–12 213.
- [28] M. Krainin, B. Curless, and D. Fox, “Autonomous generation of complete 3d object models using next best view manipulation planning,” in *2011 IEEE International Conference on Robotics and Automation*, 2011, pp. 5031–5037.
- [29] D. Peralta, J. Casimiro, A. M. Nilles, J. A. Aguilar, R. Atienza, and R. Cajote, “Next-best view policy for 3d reconstruction,” in *European Conference on Computer Vision*. Springer, 2020, pp. 558–573.
- [30] S. Kriegel, C. Rink, T. Bodenmüller, and M. Suppa, “Efficient next-best-scan planning for autonomous 3d surface reconstruction of unknown objects,” *Journal of Real-Time Image Processing*, vol. 10, no. 4, pp. 611–631, 2015.
- [31] Z. Wu, S. Song, A. Khosla, X. Tang, and J. Xiao, “3d shapenets for 2.5 d object recognition and next-best-view prediction,” *arXiv preprint arXiv:1406.5670*, vol. 2, no. 4, 2014.
- [32] Y. Han, I. H. Zhan, W. Zhao, and Y.-J. Liu, “A double branch next-best-view network and novel robot system for active object reconstruction,” in *2022 International Conference on Robotics and Automation (ICRA)*, 2022, pp. 7306–7312.
- [33] T. Foissotte, O. Stasse, A. Escande, P.-B. Wieber, and A. Kheddar, “A two-steps next-best-view algorithm for autonomous 3d object modeling by a humanoid robot,” in *2009 IEEE International Conference on Robotics and Automation*, 2009, pp. 1159–1164.
- [34] B. Browatzki, V. Tikhonoff, G. Metta, H. H. Bülthoff, and C. Wallraven, “Active in-hand object recognition on a humanoid robot,” *IEEE Transactions on Robotics*, vol. 30, no. 5, pp. 1260–1269, 2014.

- [35] S. Kriegel, T. Bodenmüller, M. Suppa, and G. Hirzinger, "A surface-based next-best-view approach for automated 3d model completion of unknown objects," in *2011 IEEE International Conference on Robotics and Automation*, 2011, pp. 4869–4874.
- [36] H. Surmann, A. Nüchter, and J. Hertzberg, "An autonomous mobile robot with a 3d laser range finder for 3d exploration and digitalization of indoor environments," *Robotics and Autonomous Systems*, vol. 45, no. 3, pp. 181–198, 2003.
- [37] A. Bircher, M. Kamel, K. Alexis, H. Oleynikova, and R. Siegwart, "Receding horizon "next-best-view" planner for 3d exploration," in *2016 IEEE International Conference on Robotics and Automation (ICRA)*. IEEE, 2016, pp. 1462–1468.
- [38] H. Kato, D. Beker, M. Morariu, T. Ando, T. Matsuoka, W. Kehl, and A. Gaidon, "Differentiable rendering: A survey," *arXiv preprint arXiv:2006.12057*, 2020.
- [39] S. Zhao, W. Jakob, and T.-M. Li, "Physics-based differentiable rendering: from theory to implementation," in *ACM siggraph 2020 courses*, 2020, pp. 1–30.
- [40] P. Sundaresan, R. Antonova, and J. Bohg, "Diffcloud: Real-to-sim from point clouds with differentiable simulation and rendering of deformable objects," *arXiv preprint arXiv:2204.03139*, 2022.
- [41] J. Luo, E. Solowjow, C. Wen, J. A. Ojea, A. M. Agogino, A. Tamar, and P. Abbeel, "Reinforcement learning on variable impedance controller for high-precision robotic assembly," in *2019 International Conference on Robotics and Automation (ICRA)*. IEEE, 2019, pp. 3080–3087.
- [42] M. A. Lee, Y. Zhu, K. Srinivasan, P. Shah, S. Savarese, L. Fei-Fei, A. Garg, and J. Bohg, "Making sense of vision and touch: Self-supervised learning of multimodal representations for contact-rich tasks," in *2019 International Conference on Robotics and Automation (ICRA)*. IEEE, 2019, pp. 8943–8950.
- [43] L. Shao, T. Migimatsu, and J. Bohg, "Learning to scaffold the development of robotic manipulation skills," in *2020 IEEE International Conference on Robotics and Automation (ICRA)*. IEEE, 2020, pp. 5671–5677.
- [44] J. Xu, Z. Hou, Z. Liu, and H. Qiao, "Compare contact model-based control and contact model-free learning: A survey of robotic peg-in-hole assembly strategies," *arXiv preprint arXiv:1904.05240*, 2019.
- [45] Y. Chebotar, O. Kroemer, and J. Peters, "Learning robot tactile sensing for object manipulation," in *2014 IEEE/RSJ International Conference on Intelligent Robots and Systems*, 2014, pp. 3368–3375.
- [46] T. Tsuji, J. Ohkuma, and S. Sakaino, "Dynamic object manipulation considering contact condition of robot with tool," *IEEE Transactions on Industrial Electronics*, vol. 63, no. 3, pp. 1972–1980, 2016.
- [47] J. Silvério, G. Clivaz, and S. Calinon, "A laser-based dual-arm system for precise control of collaborative robots," in *2021 IEEE International Conference on Robotics and Automation (ICRA)*. IEEE, 2021, pp. 9183–9189.
- [48] S. Huang, Y. Yamakawa, T. Senoo, and M. Ishikawa, "Robotic needle threading manipulation based on high-speed motion strategy using high-speed visual feedback," in *2015 IEEE/RSJ International Conference on Intelligent Robots and Systems (IROS)*, 2015, pp. 4041–4046.
- [49] H. Kim, Y. Ohmura, and Y. Kuniyoshi, "Gaze-based dual resolution deep imitation learning for high-precision dexterous robot manipulation," *IEEE Robotics and Automation Letters*, vol. 6, no. 2, pp. 1630–1637, 2021.
- [50] A. Dai, M. Nießner, M. Zollöfer, S. Izadi, and C. Theobalt, "Bundlefusion: Real-time globally consistent 3d reconstruction using on-the-fly surface re-integration," *ACM Transactions on Graphics 2017 (TOG)*, 2017.
- [51] S. Izadi, D. Kim, O. Hilliges, D. Molyneaux, R. Newcombe, P. Kohli, J. Shotton, S. Hodges, D. Freeman, A. Davison, and A. Fitzgibbon, "Kinectfusion: Real-time 3d reconstruction and interaction using a moving depth camera," in *UIST '11 Proceedings of the 24th annual ACM symposium on User interface software and technology*. ACM, October 2011, pp. 559–568.
- [52] G. Thomas, M. Chien, A. Tamar, J. A. Ojea, and P. Abbeel, "Learning robotic assembly from cad," in *2018 IEEE International Conference on Robotics and Automation (ICRA)*. IEEE, 2018, pp. 3524–3531.
- [53] J. Zhang, Z. Wan, and J. Liao, "Adaptive joint optimization for 3d reconstruction with differentiable rendering," *IEEE Transactions on Visualization and Computer Graphics*, 2022.
- [54] K. He, G. Gkioxari, P. Dollár, and R. Girshick, "Mask r-cnn," in *2017 IEEE International Conference on Computer Vision (ICCV)*, 2017, pp. 2980–2988.
- [55] H. Fan, H. Su, and L. J. Guibas, "A point set generation network for 3d object reconstruction from a single image," in *Proceedings of the IEEE conference on computer vision and pattern recognition*, 2017, pp. 605–613.
- [56] T. Haarnoja, A. Zhou, P. Abbeel, and S. Levine, "Soft actor-critic: Off-policy maximum entropy deep reinforcement learning with a stochastic actor," in *International conference on machine learning*. PMLR, 2018, pp. 1861–1870.
- [57] A. Rodríguez, R. Parr, and D. Koller, "Reinforcement learning using approximate belief states," in *Proceedings of the 12th International Conference on Neural Information Processing Systems*, ser. NIPS'99. Cambridge, MA, USA: MIT Press, 1999, p. 1036–1042.
- [58] S. Ross, G. Gordon, and D. Bagnell, "A reduction of imitation learning and structured prediction to no-regret online learning," in *Proceedings of the Fourteenth International Conference on Artificial Intelligence and Statistics*, ser. Proceedings of Machine Learning Research, G. Gordon, D. Dunson, and M. Dudík, Eds., vol. 15. Fort Lauderdale, FL, USA: PMLR, 11–13 Apr 2011, pp. 627–635. [Online]. Available: <https://proceedings.mlr.press/v15/ross11a.html>
- [59] E. Coumans and Y. Bai, "Pybullet, a python module for physics simulation for games, robotics and machine learning," <http://pybullet.org>, 2016–2021.
- [60] S. Fujimoto, H. Hoof, and D. Meger, "Addressing function approximation error in actor-critic methods," in *International conference on machine learning*. PMLR, 2018, pp. 1587–1596.